pubs.acs.org/Biomac

Article

Glycan-Driven Formation of Raft-Like Domains with Hierarchical Periodic Nanoarrays on Dendrimersome Synthetic Cells

Published as part of Biomacromolecules virtual special issue "Functional Compartmentalized Polymeric Systems—In Honor of Wolfgang Meier".

Anna M. Wagner, Nina Yu. Kostina, Qi Xiao, Michael L. Klein, Virgil Percec,* and Cesar Rodriguez-Emmenegger*

Cite This: *Biomacromolecules* 2024, 25, 366−378

Read Online

ACCESS | Metrics & More | Article Recommendations | Supporting Information

ABSTRACT: The accurate spatial segregation into distinct phases within cell membranes coordinates vital biochemical processes and functionalities in living organisms. One of nature's strategies to localize reactivity is the formation of dynamic raft domains. Most raft models rely on liquid-ordered L_0 phases in a liquid-disordered L_d phase lacking correlation and remaining static, often necessitating external agents for phase separation. Here, we introduce a synthetic system of bicomponent glycodendrimersomes coassembled from Janus dendrimers and Janus glycodendrimers (JGDs), where lactose−lactose interactions exclusively drive lateral organization. This mechanism results in modulated phases across two length scales, yielding raft-like microdomains featuring nanoarrays at the nanoscale. By varying the density of lactose and molecular architecture of JGDs, the nanoarray type and size, shape, and spacing of the domains were controlled. Our findings offer insight into the potential primordial origins of rudimentary raft domains and highlight the crucial role of glycans within the glycocalyx.

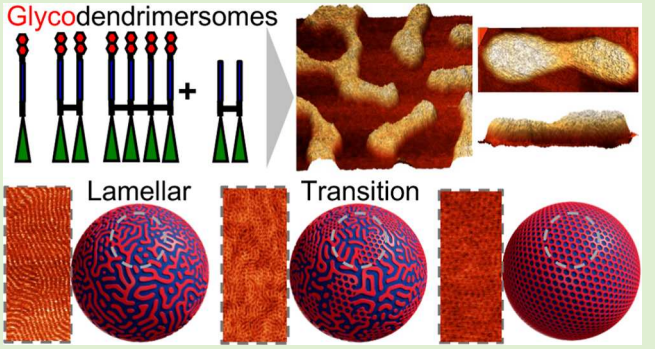

1. INTRODUCTION

The intricate lateral organization of cell membranes allows for the precise orchestration of complex biochemical processes necessary for life to unfold. Among the myriad mechanisms that govern cellular membrane organization, phase separation has emerged as a fascinating phenomenon.[1,2] The vast compositional variety in cell membranes gives rise to the ability of components to phase separate into nano- and microdomains.[3] A specific category of lipid nanodomains are raft domains, which form by the enrichment of sterols and phosphate- and glycan-based sphingolipids.[4] Raft domains are heterogeneous and dynamic subcompartments that regulate cellular functions ranging from signal transduction pathways to cell adhesion to migration to protein sorting to apoptosis.[4−6] Their size ranges from the nanoscale (10−200 nm) to the microscale (>300 nm) by clustering via protein−protein or protein−lipid interactions.[4] The undeniable significance of rafts has spurred extensive research efforts.[6−8] On one hand, efforts have been geared to elucidate the elusive and dynamic nature of rafts.[2,6,9] On the other hand, their importance as relay station for reactivity has propelled research to mimic their functionality in minimal[2,5,10,11] or synthetic systems[1,8,12−18] and utilized them to gear the insertion of channel proteins and other functional components. This lateral organization, similar to rafts, has been achieved and studied in cell membrane mimics such as liposomes,[12,19−22] polymersomes from block or graft copolymers,[14,17,18,23,24] as well as hybrid systems of lipids and polymers[15,25−29] or lipids and proteins.[22] Moreover, these domains were employed to specifically target proteins[15,21,22,30] and synthetic macromolecules.[24]

The thermodynamic driving force behind phase separation in vesicle membranes may be encoded in the molecular structure and topology of the amphiphile. Incompatibilities in the hydrophobic region of the multicomponent membrane may arise from hydrophobic mismatch due to variations in the alkyl tail length,[30−33] differences in the size of the hydrophobic block or chemistry,[14] or disparities in the ability to conform to more organized phases.[34−38] Additionally, the preferential aggregation of the hydrophilic parts of one of the components,

Received: September 25, 2023
Revised: November 22, 2023
Accepted: November 28, 2023
Published: December 8, 2023

https://doi.org/10.1021/acs.biomac.3c01027
Biomacromolecules 2024, 25, 366−378

mediated by ionic bridges with multivalent ions[23,39] or hydrogen bonding between glycans,[8] have also been explored as a means to induce phase separation. Furthermore, the mismatch in the curvature of the amphiphiles can result in curvature energies that drive the system toward two fully separated phases.[25,28,40]

The majority of the models mentioned above typically yield two entirely uncorrelated phases, most commonly a liquid-ordered (L_o) domain within a liquid-disordered (L_d) environment. These domains may fuse into a single large domain or remain stable. Their stability arises from the interplay of line tension and the elastic energy.[20,41,42] Line tension, the energy cost associated with the line boundary between the phases, is reduced by coalescence of the domains. However, the growth is accompanied by an increasing curvature energy due to the mismatch of curvature between the two phases.[20,41,42] Thus, the coalescence and growth become stalled when the energy gain by increasing the domain size is smaller than the increase in curvature energy.[43] Various other factors, including electrostatic forces, dipole interactions, and tension, can also impede domain coalescence resulting in two completely uncorrelated phases that affect membrane dynamics.[19,44−48] However, in nature, a delicate balance exists between these phases, resulting in their correlation and formation of more complex and dynamic patterns.[49−51] These homogeneous patterns, characterized by periodic variations in order parameters such as thickness, composition, density, and orientation, are referred to as modulated phases.[52] Modulated phases have been observed in both single-component lipid membranes, such as the ripple phase,[53−56] and in multicomponent membranes, where they can manifest in diverse shapes, including honeycomb patterns with hexagonal organization or the formation of stripes.[51,57]

In our previous work, we demonstrated the formation of bilayer membranes featuring modulated phases, including lamellar and hexagonal nanoarrays, by segregation of glycan moieties within the hydrophilic fragment of the amphiphiles.[58−60] To achieve these nanoarrays, we employed new synthetic alternatives to natural lipids known as amphiphilic Janus dendrimers (JDs).[61−63] Broad libraries of JDs have been synthesized to study the biological mechanism involved in cellular recognition, drug and gene delivery, and nanomedicine.[64−68] JDs consist of hydrophilic and hydrophobic dendrons linked to opposite sides of a core unit, offering precise control over membrane properties such as flexibility, lateral mobility, thickness, and stability, mimicking cell membranes effectively.[61,63,69,70] We utilized Janus glycodendrimers (JGDs), wherein linear or branched oligosaccharides were diluted in a defined way among tri(ethylene oxide) (3EO) units in the hydrophilic dendrons within one molecule to investigate glycan−lectin interactions.[58−60,71−77] We discovered that the assembly of these sequence-defined JGDs resulted in cell-membrane mimics featuring nanoarrays of glycan moieties organized in lamellar or hexagonal patterns with significantly enhanced glycan reactivity compared to that observed in GDSs where glycans densely packed and resulted in flat and uniform membranes without nanoarrays.[58,59] The nanoarray formation in monocomponent membranes was programmed by the composition of hydrophilic moieties, i.e., the ratio of glycan:3EO. Nevertheless, this discovery prompted us to explore the potential for achieving and tuning glycan nanoarrays within multicomponent GDS membranes. Furthermore, there is an intriguing question of whether we can extend the formation of modulated phases across both nano- and microlength scales, thereby facilitating the creation of raft domains with enhanced reactivity.

In this work, we aimed to investigate the role of glycans in driving the formation of micrometer-sized raft-like domains in GDSs. We assembled bicomponent synthetic vesicles from structural JDs and functional JGDs containing lactose (Lac) units of varying densities and molecular architectures (Figure 1A). The lateral and vertical organization of the JDs and JGDs

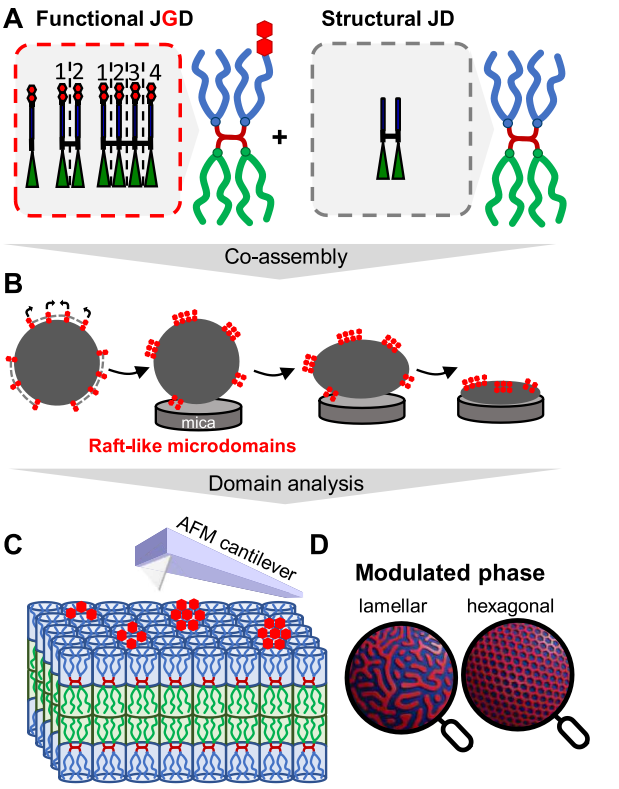

Figure 1. (A) Bicomponent system consists of a functional JGD bearing a lactose moiety and a structural JD. Due to attractive interactions between glycan groups, the formation of raft-like microdomains is programmed. (B) Preparation of bilayer films on mica support. Vesicles were formed by thin-film rehydration and then drop-casted on a mica solid support. Vesicles were dried for 24 h at ambient conditions to form bilayer stacks. (C) Characterization of supported bilayers on mica by AFM and FFT to determine bilayer thickness and molecular organization. (D) The molecular organization of glycans revealed modulated phases (lamellar and hexagonal) on the nanoscale and raft-like domains on the microscale.

was investigated by atomic force microscopy (AFM) and fast Fourier transform (FFT) on a stack of multiple overlying bilayers formed by the drying of giant vesicles on a mica support (Figure 1B−D). It should be noted that the measurements were conducted at a relative humidity of RH = 40%, which surpasses the previously reported threshold of 25%.[59] Above this threshold, the bilayer structure was maintained, suggesting that not all water was eliminated. This observation is in line with recent models demonstrating that structural water is always present if the bilayer structure is preserved.[78−80] Water molecules within the initial hydration layer persist as a structural part of the membrane, thereby forming part of its stability. Stronger dehydration would cause a disruption in the membrane.

https://doi.org/10.1021/acs.biomac.3c01027
Biomacromolecules 2024, 25, 366−378

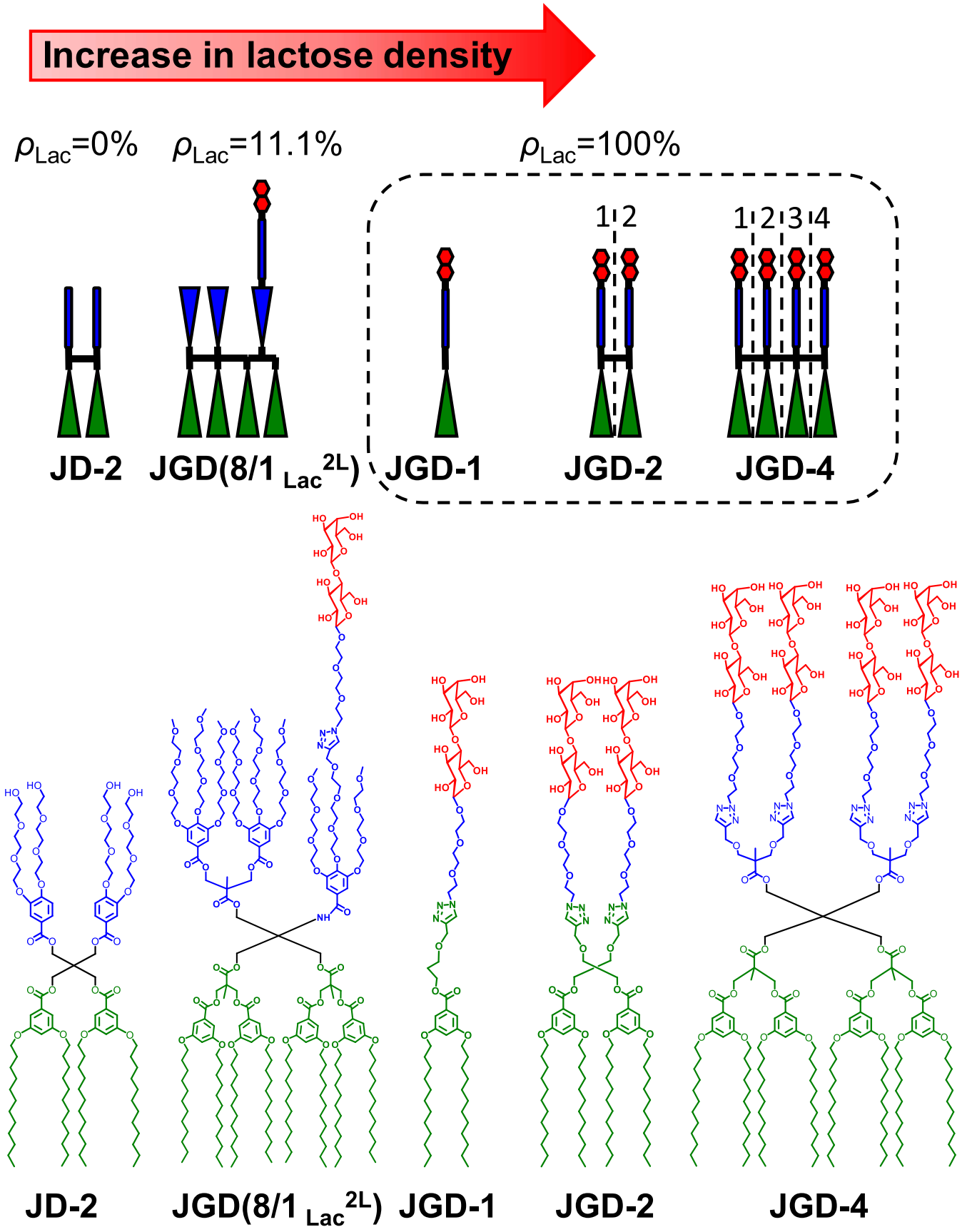

Figure 2. Architecture and chemical structures of the JDs and JGDs. The glycan density at the hydrophilic dendrons increases from the left (ρ_{Lac} = 0%) to the right (ρ_{Lac} = 100%).

https://doi.org/10.1021/acs.biomac.3c01027
Biomacromolecules 2024, 25, 366−378

By replicating an equivalent glycan dilution using two distinct molecules, it was possible to effectively program the same type of nanoarray with periodicities comparable to those observed on monocomponent membranes generated from sequence-defined JDs. We addressed the reasons behind microphase separation in mixtures containing dimers and tetramers compared to compositions with monomers, where no microscale phase separation occurred. Furthermore, we uncovered plausible reasons for why raft-like domains exhibit spatiotemporal stability without coalescing into a larger, singular domain. GDSs with raft-like domains followed a modulation in an order parameter on two different length scales: (i) first, the distribution of domains showed consistent regularities, causing a spatial modulation of the domains on the microscale, and (ii) simultaneously, the raft-like domains displayed a hierarchical periodicity and a lamellar organization of glycans within the raft on the nanoscale. Lastly, we demonstrated that glycan dilution is the key factor in controlling the type of nanoarray (lamellar and hexagonal). DSs and GDSs with "raft-like" domains are effective xenobiotic surrogates that could capture essential aspects of the cell membrane, rather than precisely replicating natural raft domains. We explored a sorting mechanism that could segregate components into functional domains, relying solely on weak interactions between hydrophilic groups. Despite its apparent simplicity, this model offers a means of localizing and enhancing the reactivity of the segregated ligands. Our findings provide insights into which basic principles governed raft domains in prebiotic life and delves into the potential impact of glycans within the glycocalyx on biological recognition.

2. EXPERIMENTAL SECTION

2.1. Materials. Anhydrous solvent THF was purchased from Acros Organics and stored over a molecular sieve. Prior to use, the solvent was filtered through 0.2 μm Teflon syringe filters by Chromafil. Fluorescent dye difluoro[2-[1-(3,5-dimethyl-2*H*-pyrrol-2-ylidene-*N*)ethyl]-3,5-dimethyl-1*H*-pyrrolato-*N*]boron (Bodipy FL) was purchased from Sigma-Aldrich. AFM cantilever OTESPA-R3 silicon probes were purchased from Bruker. Secure-Seal spacers (diameter = 13 mm, thickness = 0.12 mm) were purchased from Thermo Fisher Scientific and high precision microscope cover glasses no. 1.5H (170 ± 5 μm thickness) were provided by Marienfeld.

2.2. Synthesis of JD and JGD Library. The synthesis and characterization of all JDs and JGDs was performed as previously reported.[58,61,81]

2.3. Self-Assembly Methods for Vesicle Formation. *2.3.1. Thin-Film Rehydration.* JDs and JGDs were coassembled into giant GDSs by thin-film rehydration. Each amphiphilic component was dissolved in an organic solvent (THF, c = 10 mg mL^{-1}) and then mixed in the desired molar ratio. Additional 0.1 mol % of fluorescent dye Bodipy was added for confocal laser scanning microscopy (CLSM) characterization. The mixture (V = 30 μL) was deposited on a roughened Teflon plate and dried for t = 2 h in vacuo. The dried amphiphile film was rehydrated in Milli-Q water (V = 300 μL) at T = 60 °C for t = 12 h to obtain a vesicle dispersion with the final concentration of c = 1 mg mL^{-1}.

2.3.2. Injection Method. The injection method was employed to form small unilamellar vesicles that could be visualized by using cryogenic transmission electron microscopy (cryo-TEM). A stock solution of amphiphiles (THF, c = 10 mg mL^{-1}, V = 50 μL) was injected into Milli-Q water (V = 1 mL) and vortexed for t = 20 s. Prior to experiments, the vesicle sample was left open overnight to evaporate the remaining organic solvent.

2.4. Characterization of Vesicle Properties. *2.4.1. Atomic Force Microscopy.* Analysis of bilayer thickness and molecular organization on the surface was performed by AFM and FFT. Vesicles were drop casted onto freshly cleaved mica and dried overnight under ambient conditions (20 °C, 40% RH). During drying, the vesicles spread on the surface and broke, resulting in supported bilayers of multiple overlying bilayer stacks. Images were recorded in tapping mode using the silicon probes OTESPA-R3. Height and phase images were analyzed using Gwyddion software.

2.4.2. Confocal Laser Scanning Microscopy. For observation of vesicles in CLSM, a chamber was constructed by gluing a spacer onto a microscopy glass slide and depositing V = 20 μL of vesicle dispersion before being covered with a cover glass. Experiments were conducted on a Leica TCS SP8 confocal microscope (Wetzlar, Germany) using a 63x/1.40 glycerol-immersion objective and a PMT detector. Images were recorded with a resolution of 1024 × 1024 px and a scanning speed of 600 Hz. Images were cropped and adjusted in brightness and contrast using the Fiji software.

2.4.3. Cryogenic Transmission Electron Microscopy. Images were recorded in cryo mode at T = −168 °C and with an applied electron beam acceleration voltage of 120 kV using an in-column Omega energy filter with a CCD detector on a Zeiss Libra 120 transmission electron microscope (Oberkochen, Germany). DS and GDSs were prepared by the injection method where V = 5 μL of vesicle dispersion was deposited on plasma-treated lacey grids. The sample was flash frozen in liquid ethane using a FEI Vitrobot (Model Mark IV) plunge freezing station. Subsequently, the frozen samples were secured onto a Gatan model 910 cryo transfer specimen holder from Pleasanton, California.

3. RESULTS AND DISCUSSION

3.1. Molecular Design of JDs and JGDs. We formed GDSs by the coassembly of a JGD containing Lac in its hydrophilic dendron, which is responsible for lectin interactions, and JD-2 that allows dilution of the glycan and forms the overall chassis of the vesicle (Figure 2). All JGDs and JD-2 have the same hydrophobic 3,5-bis(dodecyloxy)benzoic ester dendron to avoid driving phase separation by a hydrophobic mismatch. JD-2 contains 4 units of tri(ethylene oxide) (3EO) in the hydrophilic dendron. For JGDs, we chose different molecular architectures. On one hand, we chose saturated JGDs, where the monomeric (1), dimeric (2), or tetrameric (4) nature (namely, JGD-1, JGD-2, and JGD-4) is indicated in the numeral of the acronym. Such JGDs have Lac in every branch of the hydrophilic dendron, thus displaying a glycan density of ρ_{glycan} = 100%. These single−single (JGD-1), twin−twin (JGD-2), and tetra−tetra (JGD-4) configurations were chosen to investigate the effect of their multiplicity in the glycan arrangement when coassembled with JD-2. On the other hand, we studied sequence-defined molecular structures designed to dilute the glycan unit within the hydrophilic dendron. Within JGD(3/1), JGD(5/1), and JGD(8/1), we indicate the ratio of tri(ethylene oxide) (3EO) units to Lac moieties in the fraction within parentheses. Such dilution of glycans results in distinct glycan surface densities of ρ_{glycan} = 25, 16.7, and 11.1%, respectively (Supporting Information Figure S1). Moreover, in the superscript, we indicate the position of the glycan as well as whether a short linker (S) with a single 3EO unit or a long linker (L) with two 3EO units was used. For instance, JGD(8/1$_{Lac}^{2S}$) features a short linker comprising a single 3EO unit (designated as "S") at the second position. Conversely, JGD(8/1$_{Lac}^{2L}$) contains a long linker, consisting of two 3EO units (designated as "L"). All of the selected sequence-defined JGDs form glycan nanoarrays (Supporting Information Figure S2).

3.2. Structural Analysis of GDS Membranes Assembled from Single−Single JGD-1 and JD-2. We examined the molecular organization of GDS membranes

https://doi.org/10.1021/acs.biomac.3c01027
Biomacromolecules 2024, 25, 366−378

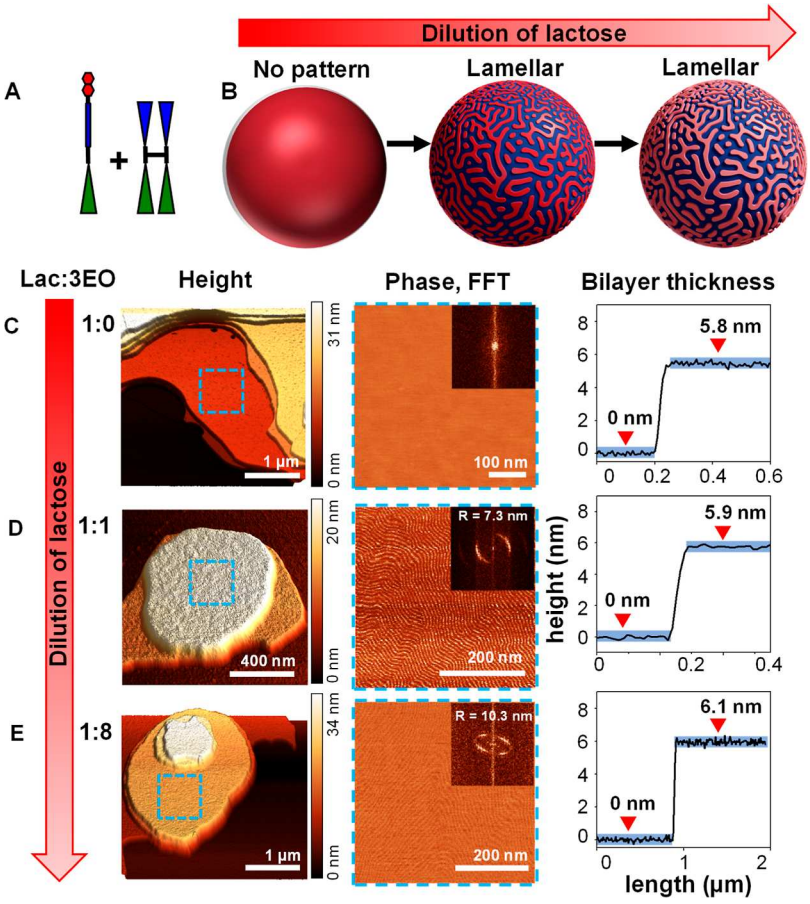

Figure 3. Membrane and Lac organization on JGD-1/JD-2 membranes was studied by AFM. (A) Schematic representation of the molecular architecture. (B) Scheme of evolution of the Lac topology in GDS's membrane with increasing dilution of Lac. Flat uniform membranes were observed for pure JGD-1, while lamellar nanoarrays with increasing prominence emerged with increasing dilution (reduction of Lac:3EO). (C–E) Three-dimensional representation of the bilayer stack height of GDSs (left), two-dimensional phase image of the area within the blue dashed square in the height image (middle) with corresponding FFT analysis (middle inset), and bilayer height determination from AFM (right). The compositions are characterized by their Lac:3EO ratio with increasing dilution of lactose from top to bottom.

resulting from the coassembly of JD-2 and JGD-1, the smallest JGD having a single–single architecture, using AFM and FFT analyses (Figure 3). All compositions resulted in the formation of giant vesicles (Supporting Information Figure S4). Compositions with Lac resulted in multilamellar vesicles, likely due to interbilayer hydrogen bonding, while pure JD-2 primarily formed unilamellar vesicles.

We varied the ratio of both components to achieve Lac:3EO ratios of 1:0, 1:1, and 1:8. In the case of monocomponent systems of JD-2 or JGD-1 (Lac:3EO = 1:0) deposited on mica, the topography images revealed flat and entirely uniform membranes (Figures 3C and S3, Supporting Information). However, the introduction of JD-2 to the GDS membrane resulted in topographies displaying alternating heights, forming lamellar nanoarrays for the studied mixtures (Lac:3EO = 1:1 and 1:8, Figure 3D,E). Notably, similar lamellar nanoarrays have previously been observed in monocomponent GDSs formed from sequence-defined JGDs containing glycan residues and 3EO within a single molecule, with glycan:3EO ratios comparable to those used in this study (Supporting Information Figure S2).[58−60] Thus, the formation of these nanoarrays appears to be regulated by the glycan:3EO ratio, irrespective of whether they are part of the same molecule or two distinct miscible components.

We further analyzed the nanoarrays by determining the membrane thickness (d) within three independent vesicle preparations in triplicate for each sample using AFM, periodicity (R) using FFT, and the mean peak-to-valley difference in height ($\bar{\Delta}$) determined from the height profiles (Supporting Information Table S1). The resulting membrane thicknesses were measured at $d_{1:1}$ = 5.9 ± 0.1 nm and $d_{1:8}$ = 6.1 ± 0.1 nm (Supporting Information Figures S7 and S8). Thus, all of the membranes exhibited a slight increase in thickness compared to those assembled from a single component ($d_{JGD\text{-}1}$ = 5.8 ± 0.1 nm and $d_{JD\text{-}2}$ = 5.2 nm in Figures 3C and S3A, Supporting Information). The periodicity and peak-to-valley height difference of the lamellar nanoarrays also exhibited an upward trend as Lac was diluted, with values shifting from $R_{1:1}$ = 7.3 nm to $R_{1:8}$ = 10.3 nm and from $\bar{\Delta}_{1:1}$ = (0.33 ± 0.06) nm to $\bar{\Delta}_{1:8}$ = (0.43 ± 0.02) nm (Supporting Information Figure S9). Notably, these $\bar{\Delta}$ values, while within the same order of magnitude, were slightly lower than the thickness difference observed between monocomponent membranes $\bar{\Delta}_{JGD\text{-}1–JD\text{-}2}$ = 5.8–5.2 nm = 0.6 nm, suggesting the coexistence of both JGD-1 and JD-2 within all regions of the membrane. The observed changes in periodicity and peak-to-valley difference of the nanoarray are consistent with similar lamellar morphologies reported in other systems where the formation of a modulated phase occurs.[51,52,82] In these systems, the order parameter was

https://doi.org/10.1021/acs.biomac.3c01027
Biomacromolecules 2024, 25, 366−378

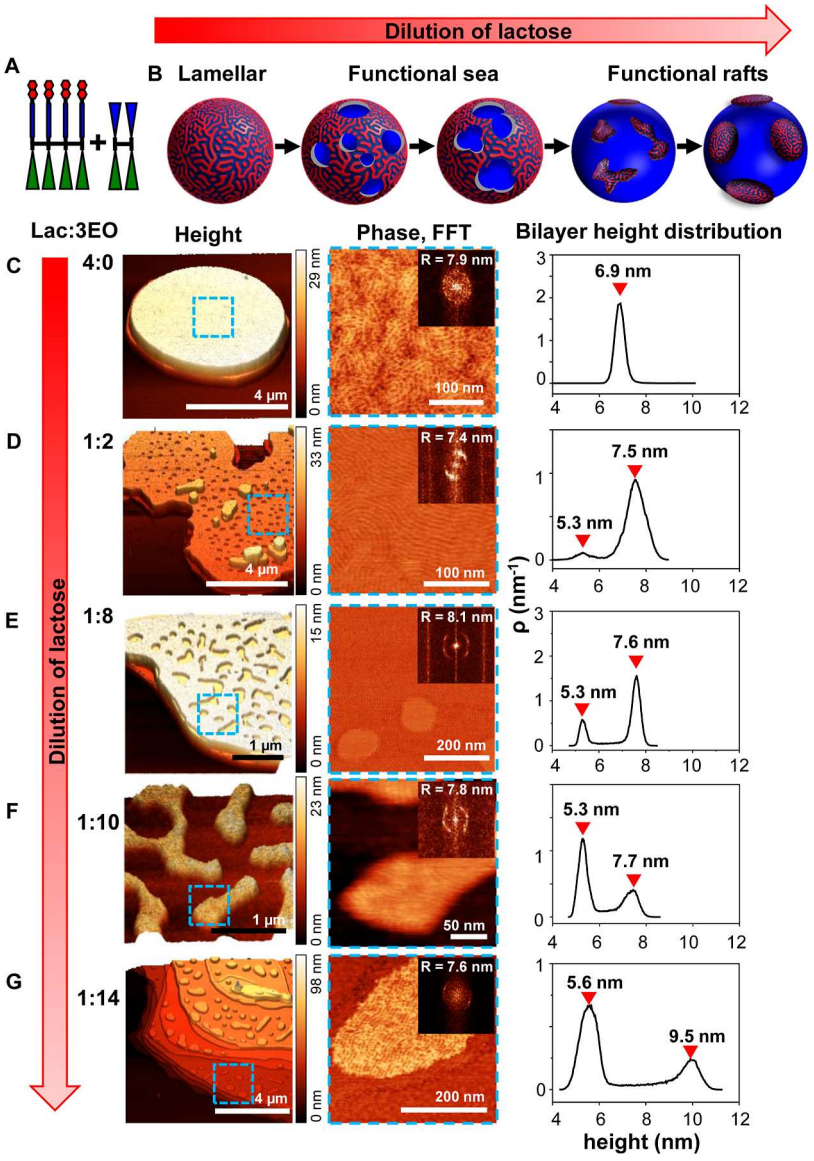

Figure 4. Structural analysis of GDS membranes assembled from tetra−tetra JGD-4 with twin−twin JD-2. (A) Scheme of the molecular architecture. (B) Scheme of the evolution of the Lac topology in GDS's membrane with increasing dilution of Lac depicting the evolution of nanoarrays as well as the formation of raft-like domains. Dilution with JD-2 created nonfunctional concave dimples with a surrounding functional sea, while a higher dilution of lactose led to the formation of functional raft-like microdomains surrounded by a nonfunctional sea. Such domains became rounder with a further increase of the JD-2 concentration. (C−G) Three-dimensional representation of the bilayer stack height of GDSs (left), two-dimensional phase image of the area within the blue dashed square in the height image (middle) with corresponding FFT analysis (middle inset), and bilayer height distribution from AFM (right). The compositions are characterized by their Lac:3EO ratio with increasing dilution of Lac from top to bottom.

modulated by external factors, including temperature, pressure, and composition.[51,52,82] On the other hand, in our bicomponent systems, the emergence of a modulated phase featuring a periodic lamellar pattern may arise from the competition between short-range attractive forces among glycans and long-range repulsion induced by membrane curvature. A plausible explanation lies in the ability to establish intermolecular hydrogen bonds among glycan residues. The formation of hydrogen bonds among Lac molecules promotes the clustering of glycans to optimize their interactions, resulting in the complete microphase separation of the JGD-1- and JD-2-rich phases. However, the cumulative effect of hydrogen bonding within the JGD-1 phase also causes compression of the interfacial area, creating an energetically unfavorable mismatch with the curvature of JD-2 domains. Thus, the competing curvature energies prevent microphase separation by inducing the breakdown of these microdomains into a periodic nanoarray structure, effectively preventing membrane bending.

3.3. Structural Analysis of GDS Membranes Assembled from Dimers and Tetramers of JGD-1 with JD-2 and the Emergence of Raft-Like Domains. Here, we examined the effect of oligomerizing the monomer units containing the glycan on the evolution of the structural features of GDS membranes. For this, we replaced JGD-1 (single−single, monomeric) for JGD-4 (tetra−tetra, Supporting Information Table S2) and JGD-2 (twin−twin, Supporting

https://doi.org/10.1021/acs.biomac.3c01027
Biomacromolecules 2024, 25, 366−378

Information Table S3), which respectively represent a covalent tetramer and dimer of JGD-1.

Figures 4 and 5 present an overview of the membrane organization in GDS assembled from JGD-4/JD-2 and JGD-2/JD-2 across a range of compositions, respectively. Similarly, for JGD-1, the monocomponent membranes assembled from JGD-2 were flat and uniform, displaying no nanoarray (Supporting Information Figure S3B). In contrast, in the monocomponent membranes self-assembled from pure JGD-4, we observed the emergence of a lamellar nanoarray characterized by periodic oscillations of the bilayer height spatially separated with a periodicity of $R_{JGD\text{-}4}$ = 7.9 nm (Figure 4C). This behavior is in contrast with the flat and uniform membrane topography observed in pure JGD-1 assemblies as well as in JGD-1 bearing mannose residues.[59] The generation of lamellar nanoarrays in membranes of JGD-4 may arise from the formation of a modulated phase as a result of the competition between attractive and repulsive interactions. Lac residues will tend to cluster to maximize the number of hydrogen bonds, which concomitantly compresses the interface and requires adopting a nonzero spontaneous curvature. The higher molecular rigidity of the JGD-4 tetramer would oppose this change in curvature more strongly than JGD-2 and JGD-1, resulting in a long-range repulsive interaction that breaks the Lac clusters leading to a lamellar nanoarray. Similar modulated phases have been observed in natural phospholipids.[53−56]

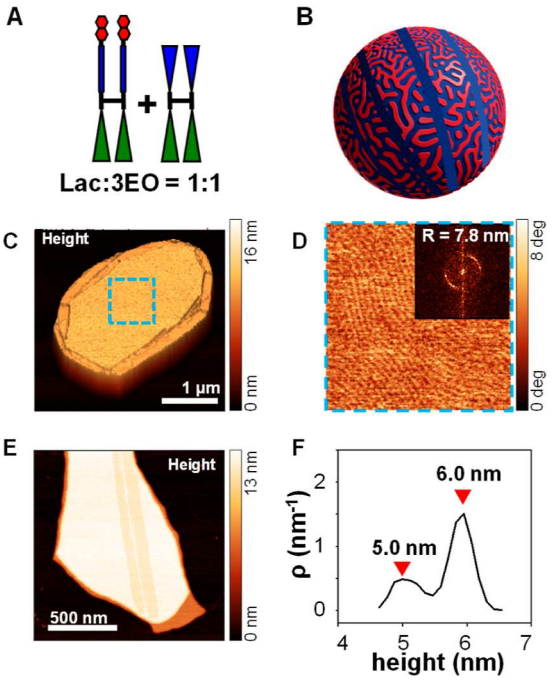

Figure 5. Microphase separation with faceted stripe domains. (A) GDSs are based on a bicomponent system of twin−twin JGD-2 and twin−twin JD-2 with the Lac:3EO ratio of 1:1. (B) Schematic representation of a functional sea with lamellar nanoarrays where faceted stripe domains are embedded. (C) Three-dimensional representation of the bilayer stack height where (D) a modulated phase with lamellar nanoarrays was detected. Two-dimensional phase image of the area within the blue dashed square in the height image with the corresponding FFT analysis (inset). (E,F) Analysis of the bilayer stack height with faceted domains and height distribution.

The coassembly of JGD-4 with JD-2 at high concentrations of Lac (Lac:3EO = 1:2 and 1:8) gave rise to microphase separation into a continuous phase with membrane thicknesses of 7.5 nm and a roundish discontinuous phase at 5.3 nm. The absence of membrane topographic features in the discontinuous phase and a thickness similar to that of pure JD-2 membranes (d = 5.2 nm, Supporting Information Figure S3A) indicate that the discontinuous phase is primarily composed of JD-2. On the other hand, the continuous phases were characterized by a thickness even higher than that of membranes assembled from pure JGD-4 and showed the emergence of lamellar nanoarrays. This corresponds to a model of a "functional sea" with embedded "non-functional concave dimples". The prominence and periodicity of the nanoarrays in the "functional sea" increased from $R_{1:2}$ = 7.4 nm to $R_{1:8}$ = 8.1 nm as the Lac density decreased. Notably, the thicknesses, periodicities, and trends observed within the continuous phase closely resemble those observed in the coassembly of monomeric JGD-1 and JD-2 under similar Lac:3EO ratios. The JGD-4 series features roundish domains exhibiting a diversity in both size and shape. Notably, the smallest domains (Lac:3EO = 1:2), characterized by an average size of 131 ± 36 nm, adopt a circular configuration. However, when the dilution ratio is increased to Lac:3EO = 1:8, elongated and branched domains emerged, which are indicative of typical shape instabilities.[52] These shapes may arise from the fusion of growing domains after spinodal decomposition during self-assembling.

Microphase separation was also observed when the tetramer was replaced by the dimer JGD-2 at a Lac:3EO ratio = 1:1 (Figure 5) with a continuous phase and a discontinuous phase having a stripe shape (Figure 5B,E). Similar to JGD-4, the thickness of the discontinuous phase (d = 5.0 nm) was close to that of the membranes of the nonfunctional JD-2 ($d_{JD\text{-}2}$ = 5.2 nm), while the continuous phase displayed a thickness d = 6.0 nm, which is higher than that of the monocomponent membrane of JGD-2 ($d_{JGD\text{-}2}$ = 5.9 nm, Supporting Information Figure S3B). This higher thickness is associated with the formation of a nanoarray with a periodicity of $R_{1:1}$ = 7.8 nm. A notable feature of the JGD-2/JD-2 membranes is the sharp-faceted nature of the continuous phase of the membrane and the boundary of the discontinuous phase (stripe-shaped domains). This contrasts with JGD-4's roundish domains, suggesting that the dimer JGD-2 was capable of packing into more ordered bilayers compared to the more rigid and larger JGD-4 that assembled into fluid ones.

When we increased the Lac dilution further (Lac:3EO = 1:10 and 1:14) in JGD-4/JD-2 GDSs, we observed the inversion of the composition of the phases. This is evidenced by the higher thickness (Figure 4) and the presence of nanoarrays in the discontinuous phase. Such "raft-like" domains concentrate the functional JGD-4 molecules forming lamellar nanoarrays with periodicities ($R_{1:10}$ = 7.8 and $R_{1:14}$ = 7.6) in the same range as for the lower dilutions. On the other hand, the continuous phase has thicknesses of 5.3 and 5.6 nm, suggesting that the majoritarian component was JD-2. Dilution significantly influenced the morphology of the "raft-like" domains, transitioning them from a branched to a circular shape as the Lac:3EO ratio shifted from 1:10 to 1:14. In the lower dilution, the growing domains are closer and have the propensity to fuse, giving rise to branched structures. Conversely, the higher dilution in the latter case increases the separation between growing domains, partly inhibiting

https://doi.org/10.1021/acs.biomac.3c01027
Biomacromolecules 2024, 25, 366−378

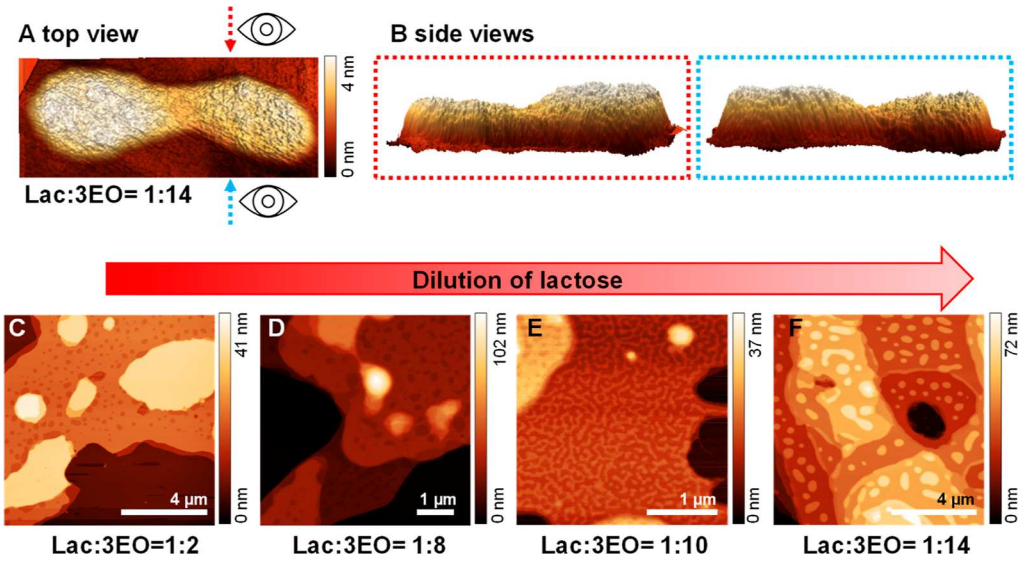

Figure 6. Microdomain shape and distribution. (A,B) Three-dimensional AFM images of a single domain in GDSs from JGD-4 and JD-2 with a Lac:3EO ratio = 1:14. The images include a top-down view (A) and side views (B) along the designated red or blue dashed lines. These three-dimensional figures show the increase in curvature of the microdomains. (C−F) Overview AFM images of microphase separation in GDSs from JGD-4 and JD-2 with increasing dilution of lactose from left to right.

fusion and consequently yielding predominantly circular domains.

Microphase separation is a powerful tool to design the surface topology of a GDS and confine the functionality to microdomains, like rafts in cell membranes. In natural cells, rafts are like functional relay stations for cellular signaling and trafficking that are generated by the interplay of nonlipid amphiphiles and functional proteins. In contrast, in the GDS membranes, only a bicomponent system was sufficient to create functional raft-like domains in which glycans organized in lamellar nanoarrays previously shown to have an increased biological activity in a mechanism alike the proposed superselectivity.[59,83−85] But why did microphase separation occur in mixtures with the dimer and tetramer but not the monomer? In addition, why did such raft-like domains not coalesce into a larger single domain? All JGDs in this work have the same glycan residue and, thereby, the same cohesive forces between them. However, the entropy loss for demixing the dimers and tetramers from JD-2 is lower than that for the JGD-1/JD-2 system, enabling the microphase separation of the formers at the expense of creating a phase boundary with line tension, as shown in Figures 4 and 5. Remarkably, these domains display a rather homogeneous shape and size and remain stable in spite of the drive of the line tension to coalesce into a single domain, i.e., macrophase separation. Consequently, long-range repulsive interactions must be at play to stall coalescence. In lipid GUVs, it has been demonstrated that fluid domains adopt dimpled morphologies.[44,45] Dimpling allows domains in proximity to repel due to the deformations of the surrounding membrane that prevent coalescence and also regulates their size since the repulsion force scales with domain area and the line tension. This purely mechanical model provided an alternative explanation to lipid rafts, which have frequently been described as liquid-ordered (L_o) domains floating within a liquid-disordered phase (L_d) and thus excluding the possibility of having fluid domains. In this study, we analyzed the topography of various domains. Figure 6A,B depicts the three-dimensional AFM images of a composition (JGD-4/JD-2, Lac:3EO = 1:14) forming raft-like domains with a bird's-eye view of a sole microdomain and side views from two distinct viewpoints. This exemplifies the unique protruding shapes of the domains concomitant with an increase in curvature that occurs as a result of dimpling.

Moreover, examination of the overview AFM topography images for each composition (Figure 6C−F) revealed that the distribution of domains exhibited consistent regularities, resulting in a spatial modulation of the domains. With increasing dilution of Lac units, we detected a transition between concave dimples, maze-like structures, and convex nipple-like protrusions. These spatial patterns where an order parameter is modulated are called modulated phases and are pervasive in nature.[49,50,52] For instance, a very similar organization at the same scale was observed in the cornea of insects across several insect species.[49] Moreover, this model implies that the raft-like domains are not uncorrelated to the surrounding phase, but that their size, shape, and spacing can be modulated by the ratio of the two components of the membrane. Thus, this is indicative of a plausible mechanism to localize reactivity in primordial cells.

3.4. Controlling the Nanoarray Formation by Composition. In previous works, the assembly of sequence-defined JGDs has been found to result in the formation of lamellar and hexagonal nanoarrays on GDS membranes from mono-, di-, and oligosaccharides sequence-defined JGDs.[58−60] The organization of glycans into nanoarrays has demonstrated an elevated biological reactivity toward glycan-binding lectins.[59] While JGD(8/1_{Lac}^{2L}) with a Lac density of ρ_{Lac} = 11.1% assembled into membranes with hexagonal nanoarrays, JGDs with a glycan density in the range of 14.3% < ρ_{glycan} < 25% organized into lamellar nanoarrays.[58,59]

Herein, we investigated the programmability of the nanoarray type by adjusting ρ_{glycan}. To achieve this, we varied the Lac:3EO ratio in a bicomponent membrane coassembled from sequence-defined JGD(8/1_{Lac}^{2L}) and JGD-1 (Figure 7, Supporting Information Table S4). Monocomponent membranes from pure JGD(8/1_{Lac}^{2L}) displayed membranes with hexagonal nanoarrays with periodicity $R_{JGD(8/1Lac}^{2L}$) = 8.0 nm and a bilayer thickness of d = 7.3 nm. In mixtures of JGD(8/

https://doi.org/10.1021/acs.biomac.3c01027
Biomacromolecules 2024, 25, 366−378

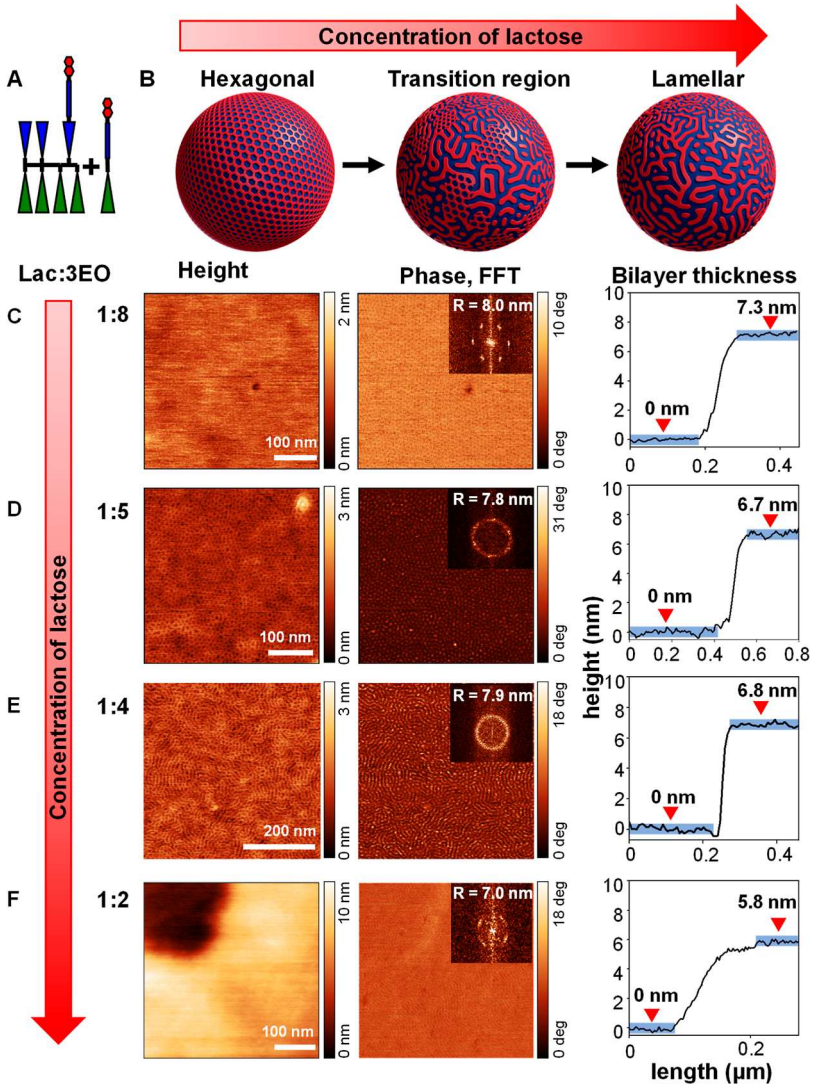

Figure 7. Controlling the type of Lac topology at GDS membranes by composition. (A) Scheme of the molecular architecture of sequence-defined JGD(8/1_{Lac}^{2L}) and single−single JGD-1 coassembled into GDSs displayed in this figure. (B) Schematic representation of the evolution of the topology of Lac with varying concentrations of the lactose by introducing JGD-1. A hexagonal nanoarray is found at the lowest density of Lac [pure JGD(8/1_{Lac}^{2L})]. With increasing concentration of lactose, a transition region displays a mixture of hexagonal and lamellar patterning, while with the highest concentration, only a lamellar organization of lactose was observed. (C−F) AFM height (left) and phase images (middle) with corresponding FFT analysis (middle inset) and bilayer height determination from AFM (right). The compositions are characterized by their Lac:3EO ratio with increasing concentration of lactose from top to bottom.

1_{Lac}^{2L}) and JGD-1 with Lac:3EO ratios of 1:5 (ρ_{Lac} = 16.7%) and 1:4 (ρ_{Lac} = 20%), we observed a transition where regions of hexagonal and lamellar nanoarrays coexisted. While the former composition was predominantly hexagonal with some lamellar regions ($R_{1:5}$ = 7.8 nm), in the latter composition, we observed an equal mixture of hexagonal and lamellar nanoarrays. Moreover, we confirmed that the nanoarrays are independent from their interaction with the mica substrate by scanning four consecutive bilayers that demonstrate identical organization of Lac units ranging in periodicity from $R_{1:4}$ = 7.2 to 7.9 nm (Supporting Information Figure S10). Moreover, both compositions exhibited similar bilayer thicknesses of $d_{1:5}$ = 6.7 nm and $d_{1:4}$ = 6.8 nm.

In our bicomponent membranes, we observed lamellar nanoarrays at slightly higher Lac ratios of ρ_{Lac} = 33.3% and Lac:3EO = 1:2 compared to monocomponent membranes from sequence-defined JGD(3/1_{Lac}) (ρ_{Lac} = 25%) (Supporting Information Figure S2). Here, we detected the lowest periodicity of $R_{1:2}$ = 7.0 nm and the smallest bilayer thickness of $d_{1:2}$ = 5.8 nm, which follows the same trend that we discussed in the previous chapters.

4. CONCLUSIONS

In this study, we investigated the role of glycans in driving the formation of micrometer-sized raft-like domains in bicomponent GDSs. By using two distinct molecules, we could produce nanoarrays with characteristics similar to those found in monocomponent membranes from sequence-defined JGDs. Such nanoarrays represent a modulated phase, a phenomenon that is ubiquitous in nature.[49,50,52] Bicomponent GDSs from the monomeric single−single JGD (JGD-1) and twin−twin JD (JD-2) resulted in lamellar nanoarrays in all of the tested ρ_{Lac}. However, replacing JGD-1 monomers with JGD-4 tetramers and JGD-2 dimers significantly impacts the phase separation behavior by altering the molecular rigidity and packing efficiency. We discovered that by only altering ρ_{Lac}, we could

https://doi.org/10.1021/acs.biomac.3c01027
Biomacromolecules 2024, 25, 366−378

produce a range of spatial arrangements within the membranes, such as a "functional sea" containing embedded "nonfunctional concave dimples", stripe-shaped domains, as well as a transition between concave dimples, maze-like structures, and convex nipple-like protrusions. These findings emphasize the emergence of microscale modulated phases and introduce a model of "raft-like domains" with hierarchical periodicity. Since these raft-like domains are correlated with the surrounding phase, their size, shape, and spacing can be adjusted by the ratio of the two components of the membrane.

Our findings demonstrate that functional raft-like domains can emerge through weak interactions between glycans within hydrophilic headgroups of JGDs without the need for hydrophobic mismatch, crystallization, or additional compounds such as cholesterol or proteins. We present a mechanism for creating rudimentary raft domains that replicate key principles that could have governed the formation of raft domains localizing reactivity in primordial cells without the need for the complexity of contemporary cell membranes. This work describes a potential mechanism for regulating the spatial arrangement of glycolipids within the glycocalyx, which plays a critical role in controlling cellular interactions, processes, and glycan−lectin interactions, providing insight into the connection between supramolecular assembly and biological recognition.

■ ASSOCIATED CONTENT

Supporting Information

The Supporting Information is available free of charge at https://pubs.acs.org/doi/10.1021/acs.biomac.3c01027.

Chemical structures and nano-organization of sequence-defined JGDs, AFM analysis of selected monocomponent DSs and GDSs, summary of compositions in bicomponent systems and the respective membrane properties determined from AFM, studies on vesicles using CLSM and cryo-TEM, statistical analysis of the bilayer thickness, peak-to-valley distance in lamellar nanoarrays, and characterization of the interaction with the mica substrate (PDF)

■ AUTHOR INFORMATION

Corresponding Authors

Virgil Percec − *Roy & Diana Vagelos Laboratories, Department of Chemistry, University of Pennsylvania, Philadelphia, Pennsylvania 19104-6323, United States;* orcid.org/0000-0001-5926-0489; Email: percec@sas.upenn.edu

Cesar Rodriguez-Emmenegger − *DWI-Leibniz Institute for Interactive Materials, Aachen 52074, Germany; Institute for Bioengineering of Catalonia (IBEC), The Barcelona Institute of Science and Technology (BIST), Barcelona 08028, Spain; Institució Catalana de Recerca i Estudis Avançats (ICREA), Barcelona 08028, Spain;* orcid.org/0000-0003-0745-0840; Email: crodriguez@ibecbarcelona.eu

Authors

Anna M. Wagner − *DWI-Leibniz Institute for Interactive Materials, Aachen 52074, Germany; Institute of Technical and Macromolecular Chemistry, RWTH Aachen University, Aachen 52074, Germany;* orcid.org/0000-0002-2489-2803

Nina Yu. Kostina − *Institute for Bioengineering of Catalonia (IBEC), The Barcelona Institute of Science and Technology (BIST), Barcelona 08028, Spain*

Qi Xiao − *Roy & Diana Vagelos Laboratories, Department of Chemistry, University of Pennsylvania, Philadelphia, Pennsylvania 19104-6323, United States; Institute of Computational Molecular Science, Temple University, Philadelphia, Pennsylvania 19122, United States;* orcid.org/0000-0002-6470-0407

Michael L. Klein − *Institute of Computational Molecular Science, Temple University, Philadelphia, Pennsylvania 19122, United States;* orcid.org/0000-0002-0027-9262

Complete contact information is available at: https://pubs.acs.org/10.1021/acs.biomac.3c01027

Notes

The authors declare no competing financial interest.

■ ACKNOWLEDGMENTS

This work was supported by the grant PID2022-142598OB-I00 funded by MCIN/AEI/10.13039/501100011033, ERDF A way of making Europe, H2020-NMBP-TRIND-2018, EVPRO (Development of Extracellular Vesicles loaded hydrogel coatings with immunomodulatory activity for Promoted Regenerative Osseointegration of revision endoprosthesis) grant 814495-2, a Ramon y Cajal Fellowship (N.Y.K.) grant RYC2021-032317-I funded by MCIN/AEI/10.13039/501100011033, and the "European Union NextGenerationEU/PRTR". V.P. acknowledges support by the National Science Foundation (DMR-1807127, DMR-1720530 and DMR-2104554) and the P. Roy Vagelos Chair at Penn. Moreover, authors acknowledge the support of the RWTH University via the calls Innovation Sprint 2021 (project ANVIVES) as part of the "Exzellenz Start-up Center NRW" initiative and ERS Seed Fund Projects SFSynt003 and SFSynt005. IBEC is a member of the CERCA program. M.L.K. thanks HRH Sheikh Saud for the award of a Sheikh Saqr Research Fellowship. The authors thank Anton Joseph for the preparation of schemes of three-dimensional vesicles with nanoarrays.

■ REFERENCES

(1) Bagatolli, L. A. To see or not to see: lateral organization of biological membranes and fluorescence microscopy. *Biochim. Biophys. Acta* **2006**, *1758*, 1541−1556.

(2) Sezgin, E.; Levental, I.; Mayor, S.; Eggeling, C. The mystery of membrane organization: composition, regulation and roles of lipid rafts. *Nat. Rev. Mol. Cell Biol.* **2017**, *18*, 361−374.

(3) Harayama, T.; Riezman, H. Understanding the diversity of membrane lipid composition. *Nat. Rev. Mol. Cell Biol.* **2018**, *19*, 281−296.

(4) Pike, L. J. Rafts defined: a report on the Keystone symposium on lipid rafts and cell function. *J. Lipid Res.* **2006**, *47*, 1597−1598.

(5) Munro, S. Lipid rafts: elusive or illusive? *Cell* **2003**, *115*, 377−388.

(6) Lingwood, D.; Simons, K. Lipid Rafts As a Membrane-Organizing Principle. *Science* **2010**, *327*, 46−50.

(7) Simons, K.; Ikonen, E. Functional rafts in cell membranes. *Nature* **1997**, *387*, 569−572.

(8) Cebecauer, M.; Amaro, M.; Jurkiewicz, P.; Sarmento, M. J.; Šachl, R.; Cwiklik, L.; Hof, M. Membrane Lipid Nanodomains. *Chem. Rev.* **2018**, *118*, 11259−11297.

(9) Gaus, K.; Gratton, E.; Kable, E. P. W.; Jones, A. S.; Gelissen, I.; Kritharides, L.; Jessup, W. Visualizing lipid structure and raft domains

in living cells with two-photon microscopy. *Proc. Natl. Acad. Sci. U.S.A.* **2003**, *100*, 15554−15559.
(10) Levental, I.; Levental, K. R.; Heberle, F. A. Lipid Rafts: Controversies Resolved, Mysteries Remain. *Trends Cell Biol.* **2020**, *30*, 341−353.
(11) Pike, L. J. Lipid rafts: heterogeneity on the high seas. *Biochem. J.* **2004**, *378*, 281−292.
(12) Veatch, S. L.; Keller, S. L. Separation of Liquid Phases in Giant Vesicles of Ternary Mixtures of Phospholipids and Cholesterol. *Biophys. J.* **2003**, *85*, 3074−3083.
(13) Veatch, S. L.; Keller, S. L. Seeing spots: Complex phase behavior in simple membranes. *Biochim. Biophys. Acta, Mol. Cell Res.* **2005**, *1746*, 172−185.
(14) Lopresti, C.; Massignani, M.; Fernyhough, C.; Blanazs, A.; Ryan, A. J.; Madsen, J.; Warren, N. J.; Armes, S. P.; Lewis, A. L.; Chirasatitsin, S.; Engler, A. J.; Battaglia, G. Controlling Polymersome Surface Topology at the Nanoscale by Membrane Confined Polymer/Polymer Phase Separation. *ACS Nano* **2011**, *5*, 1775−1784.
(15) Kowal, J.; Wu, D.; Mikhalevich, V.; Palivan, C. G.; Meier, W. Hybrid Polymer-Lipid Films as Platforms for Directed Membrane Protein Insertion. *Langmuir* **2015**, *31*, 4868−4877.
(16) Mouritsen, O. G.; Bagatolli, L. A. Lipid domains in model membranes: a brief historical perspective. *Essays Biochem.* **2015**, *57*, 1−19.
(17) Rideau, E.; Wurm, F. R.; Landfester, K. Membrane Engineering: Phase Separation in Polymeric Giant Vesicles. *Small* **2020**, *16*, 1905230.
(18) Almadhi, S.; Forth, J.; Rodriguez-Arco, L.; Duro-Castano, A.; Williams, I.; Ruiz-Perez, L.; Battaglia, G. Bottom-Up Preparation of Phase-Separated Polymersomes. *Macromol. Biosci.* **2023**, *23*, 2300068.
(19) Baumgart, T.; Hess, S. T.; Webb, W. W. Imaging coexisting fluid domains in biomembrane models coupling curvature and line tension. *Nature* **2003**, *425*, 821−824.
(20) Baumgart, T.; Das, S.; Webb, W. W.; Jenkins, J. T. Membrane Elasticity in Giant Vesicles with Fluid Phase Coexistence. *Biophys. J.* **2005**, *89*, 1067−1080.
(21) Stachowiak, J. C.; Hayden, C. C.; Sanchez, M. A. A.; Wang, J.; Bunker, B. C.; Voigt, J. A.; Sasaki, D. Y. Targeting Proteins to Liquid-Ordered Domains in Lipid Membranes. *Langmuir* **2011**, *27*, 1457−1462.
(22) Scheve, C. S.; Gonzales, P. A.; Momin, N.; Stachowiak, J. C. Steric Pressure between Membrane-Bound Proteins Opposes Lipid Phase Separation. *J. Am. Chem. Soc.* **2013**, *135*, 1185−1188.
(23) Christian, D. A.; Tian, A.; Ellenbroek, W. G.; Levental, I.; Rajagopal, K.; Janmey, P. A.; Liu, A. J.; Baumgart, T.; Discher, D. E. Spotted vesicles, striped micelles and Janus assemblies induced by ligand binding. *Nat. Mater.* **2009**, *8*, 843−849.
(24) Sasaki, D. Y.; Zawada, N.; Gilmore, S. F.; Narasimmaraj, P.; Sanchez, M. A. A.; Stachowiak, J. C.; Hayden, C. C.; Wang, H.-L.; Parikh, A. N.; Shreve, A. P. Lipid Membrane Domains for the Selective Adsorption and Surface Patterning of Conjugated Polyelectrolytes. *Langmuir* **2013**, *29*, 5214−5221.
(25) Chemin, M.; Brun, P.-M.; Lecommandoux, S.; Sandre, O.; Le Meins, J.-F. Hybrid polymer/lipid vesicles: fine control of the lipid and polymer distribution in the binary membrane. *Soft Matter* **2012**, *8*, 2867.
(26) Dao, T. P. T.; Fernandes, F.; Er-Rafik, M.; Salva, R.; Schmutz, M.; Brûlet, A.; Prieto, M.; Sandre, O.; Le Meins, J. F. Phase Separation and Nanodomain Formation in Hybrid Polymer/Lipid Vesicles. *ACS Macro Lett.* **2015**, *4*, 182−186.
(27) Chen, D.; Santore, M. M. Hybrid copolymer-phospholipid vesicles: phase separation resembling mixed phospholipid lamellae, but with mechanical stability and control. *Soft Matter* **2015**, *11*, 2617−2626.
(28) Dao, T. P. T.; Fernandes, F.; Ibarboure, E.; Ferji, K.; Prieto, M.; Sandre, O.; Le Meins, J.-F. Modulation of phase separation at the micron scale and nanoscale in giant polymer/lipid hybrid unilamellar vesicles (GHUVs). *Soft Matter* **2017**, *13*, 627−637.
(29) Di Leone, S.; Kyropoulou, M.; Köchlin, J.; Wehr, R.; Meier, W. P.; Palivan, C. G. Tailoring a Solvent-Assisted Method for Solid-Supported Hybrid Lipid-Polymer Membranes. *Langmuir* **2022**, *38*, 6561−6570.
(30) Belluati, A.; Mikhalevich, V.; Yorulmaz Avsar, S.; Daubian, D.; Craciun, I.; Chami, M.; Meier, W. P.; Palivan, C. G. How Do the Properties of Amphiphilic Polymer Membranes Influence the Functional Insertion of Peptide Pores? *Biomacromolecules* **2020**, *21*, 701−715.
(31) Jensen, M. Ø.; Mouritsen, O. G. Lipids do influence protein function-the hydrophobic matching hypothesis revisited. *Biochim. Biophys. Acta* **2004**, *1666*, 205−226.
(32) García-Sáez, A. J.; Chiantia, S.; Schwille, P. Effect of Line Tension on the Lateral Organization of Lipid Membranes. *J. Biol. Chem.* **2007**, *282*, 33537−33544.
(33) Heberle, F. A.; Petruzielo, R. S.; Pan, J.; Drazba, P.; Kučerka, N.; Standaert, R. F.; Feigenson, G. W.; Katsaras, J. Bilayer Thickness Mismatch Controls Domain Size in Model Membranes. *J. Am. Chem. Soc.* **2013**, *135*, 6853−6859.
(34) Hjort Ipsen, J.; Karlström, G.; Mourtisen, O. G.; Wennerström, H.; Zuckermann, M. J. Phase equilibria in the phosphatidylcholine-cholesterol system. *Biochim. Biophys. Acta* **1987**, *905*, 162−172.
(35) Harder, T.; Simons, K. Caveolae, DIGs, and the dynamics of sphingolipid-cholesterol microdomains. *Curr. Opin. Cell Biol.* **1997**, *9*, 534−542.
(36) Brown, D. A.; London, E. Structure and Origin of Ordered Lipid Domains in Biological Membranes. *J. Membr. Biol.* **1998**, *164*, 103−114.
(37) Beales, P. A.; Gordon, V. D.; Zhao, Z.; Egelhaaf, S. U.; Poon, W. C. K. Solid-like domains in fluid membranes. *J. Phys.: Condens.Matter* **2005**, *17*, S3341−S3346.
(38) Momin, N.; Lee, S.; Gadok, A. K.; Busch, D. J.; Bachand, G. D.; Hayden, C. C.; Stachowiak, J. C.; Sasaki, D. Y. Designing lipids for selective partitioning into liquid ordered membrane domains. *Soft Matter* **2015**, *11*, 3241−3250.
(39) Carvalho, K.; Ramos, L.; Roy, C.; Picart, C. Giant Unilamellar Vesicles Containing Phosphatidylinositol(4,5)bisphosphate: Characterization and Functionality. *Biophys. J.* **2008**, *95*, 4348−4360.
(40) Brea, R. J.; Rudd, A. K.; Devaraj, N. K. Nonenzymatic biomimetic remodeling of phospholipids in synthetic liposomes. *Proc. Natl. Acad. Sci. U.S.A.* **2016**, *113*, 8589−8594.
(41) Lipowsky, R. Budding of membranes induced by intramembrane domains. *J. Phys. II* **1992**, *2*, 1825−1840.
(42) Jülicher, F.; Lipowsky, R. Domain-induced budding of vesicles. *Phys. Rev. Lett.* **1993**, *70*, 2964−2967.
(43) Hu, J.; Weikl, T.; Lipowsky, R. Vesicles with multiple membrane domains. *Soft Matter* **2011**, *7*, 6092.
(44) Ursell, T. S.; Klug, W. S.; Phillips, R. Morphology and interaction between lipid domains. *Proc. Natl. Acad. Sci. U.S.A.* **2009**, *106*, 13301−13306.
(45) Semrau, S.; Idema, T.; Schmidt, T.; Storm, C. Membrane-Mediated Interactions Measured Using Membrane Domains. *Biophys. J.* **2009**, *96*, 4906−4915.
(46) Hamada, T.; Kishimoto, Y.; Nagasaki, T.; Takagi, M. Lateral phase separation in tense membranes. *Soft Matter* **2011**, *7*, 9061.
(47) Rozovsky, S.; Kaizuka, Y.; Groves, J. T. Formation and spatio-temporal evolution of periodic structures in lipid bilayers. *J. Am. Chem. Soc.* **2005**, *127*, 36−37.
(48) Parthasarathy, R.; Yu, C.-H.; Groves, J. T. Curvature-Modulated Phase Separation in Lipid Bilayer Membranes. *Langmuir* **2006**, *22*, 5095−5099.
(49) Blagodatski, A.; Sergeev, A.; Kryuchkov, M.; Lopatina, Y.; Katanaev, V. L. Diverse set of Turing nanopatterns coat corneae across insect lineages. *Proc. Natl. Acad. Sci. U.S.A.* **2015**, *112*, 10750−10755.
(50) Turing, A. M. The chemical basis of morphogenesis. *Philos. Trans. R. Soc., B* **1952**, *237*, 37−72.

https://doi.org/10.1021/acs.biomac.3c01027
Biomacromolecules 2024, 25, 366−378

(51) Goh, S. L.; Amazon, J. J.; Feigenson, G. W. Toward a better raft model: modulated phases in the four-component bilayer, DSPC/DOPC/POPC/CHOL. *Biophys. J.* **2013**, *104*, 853−862.
(52) Seul, M.; Andelman, D. Domain Shapes and Patterns: The Phenomenology of Modulated Phases. *Science* **1995**, *267*, 476−483.
(53) Carlson, J. M.; Sethna, J. P. Theory of the ripple phase in hydrated phospholipid bilayers. *Phys. Rev. A* **1987**, *36*, 3359−3374.
(54) Kranenburg, M.; Smit, B. Phase Behavior of Model Lipid Bilayers. *J. Phys. Chem. B* **2005**, *109*, 6553−6563.
(55) Akabori, K.; Nagle, J. F. Structure of the DMPC lipid bilayer ripple phase. *Soft Matter* **2015**, *11*, 918−926.
(56) Tardieu, A.; Luzzati, V.; Reman, F. C. Structure and polymorphism of the hydrocarbon chains of lipids: A study of lecithin-water phases. *J. Mol. Biol.* **1973**, *75*, 711−733.
(57) Konyakhina, T. M.; Goh, S. L.; Amazon, J.; Heberle, F. A.; Wu, J.; Feigenson, G. W. Control of a nanoscopic-to-macroscopic transition: modulated phases in four-component DSPC/DOPC/POPC/Chol giant unilamellar vesicles. *Biophys. J.* **2011**, *101*, L8−L10.
(58) Rodriguez-Emmenegger, C.; Xiao, Q.; Kostina, N. Y.; Sherman, S. E.; Rahimi, K.; Partridge, B. E.; Li, S.; Sahoo, D.; Reveron Perez, A. M.; Buzzacchera, I.; Han, H.; Kerzner, M.; Malhotra, I.; Möller, M.; Wilson, C. J.; Good, M. C.; Goulian, M.; Baumgart, T.; Klein, M. L.; Percec, V. Encoding biological recognition in a bicomponent cell-membrane mimic. *Proc. Natl. Acad. Sci. U.S.A.* **2019**, *116*, 5376−5382.
(59) Kostina, N. Y.; Söder, D.; Haraszti, T.; Xiao, Q.; Rahimi, K.; Partridge, B. E.; Klein, M. L.; Percec, V.; Rodriguez-Emmenegger, C. Enhanced Concanavalin A Binding to Preorganized Mannose Nanoarrays in Glycodendrimersomes Revealed Multivalent Interactions. *Angew. Chem., Int. Ed.* **2021**, *60*, 8352−8360.
(60) Xiao, Q.; Delbianco, M.; Sherman, S. E.; Reveron Perez, A. M.; Bharate, P.; Pardo-Vargas, A.; Rodriguez-Emmenegger, C.; Kostina, N. Y.; Rahimi, K.; Söder, D.; Möller, M.; Klein, M. L.; Seeberger, P. H.; Percec, V. Nanovesicles displaying functional linear and branched oligomannose self-assembled from sequence-defined Janus glycodendrimers. *Proc. Natl. Acad. Sci. U.S.A.* **2020**, *117*, 11931−11939.
(61) Percec, V.; Wilson, D. A.; Leowanawat, P.; Wilson, C. J.; Hughes, A. D.; Kaucher, M. S.; Hammer, D. A.; Levine, D. H.; Kim, A. J.; Bates, F. S.; Davis, K. P.; Lodge, T. P.; Klein, M. L.; DeVane, R. H.; Aqad, E.; Rosen, B. M.; Argintaru, A. O.; Sienkowska, M. J.; Rissanen, K.; Nummelin, S.; Ropponen, J. Self-Assembly of Janus Dendrimers into Uniform Dendrimersomes and Other Complex Architectures. *Science* **2010**, *328*, 1009−1014.
(62) Percec, V.; Leowanawat, P.; Sun, H. J.; Kulikov, O.; Nusbaum, C. D.; Tran, T. M.; Bertin, A.; Wilson, D. A.; Peterca, M.; Zhang, S.; Kamat, N. P.; Vargo, K.; Moock, D.; Johnston, E. D.; Hammer, D. A.; Pochan, D. J.; Chen, Y.; Chabre, Y. M.; Shiao, T. C.; Bergeron-Brlek, M.; Andre, S.; Roy, R.; Gabius, H. J.; Heiney, P. A. Modular synthesis of amphiphilic Janus glycodendrimers and their self-assembly into glycodendrimersomes and other complex architectures with bioactivity to biomedically relevant lectins. *J. Am. Chem. Soc.* **2013**, *135*, 9055−9077.
(63) Sherman, S. E.; Xiao, Q.; Percec, V. Mimicking Complex Biological Membranes and Their Programmable Glycan Ligands with Dendrimersomes and Glycodendrimersomes. *Chem. Rev.* **2017**, *117*, 6538−6631.
(64) Zhang, D.; Atochina-Vasserman, E. N.; Lu, J.; Maurya, D. S.; Xiao, Q.; Liu, M.; Adamson, J.; Ona, N.; Reagan, E. K.; Ni, H.; Weissman, D.; Percec, V. The Unexpected Importance of the Primary Structure of the Hydrophobic Part of One-Component Ionizable Amphiphilic Janus Dendrimers in Targeted mRNA Delivery Activity. *J. Am. Chem. Soc.* **2022**, *144*, 4746−4753.
(65) Zhang, D.; Atochina-Vasserman, E. N.; Maurya, D. S.; Huang, N.; Xiao, Q.; Ona, N.; Liu, M.; Shahnawaz, H.; Ni, H.; Kim, K.; Billingsley, M. M.; Pochan, D. J.; Mitchell, M. J.; Weissman, D.; Percec, V. One-Component Multifunctional Sequence-Defined Ionizable Amphiphilic Janus Dendrimer Delivery Systems for mRNA. *J. Am. Chem. Soc.* **2021**, *143*, 12315−12327.
(66) Zhang, D.; Atochina-Vasserman, E. N.; Maurya, D. S.; Liu, M.; Xiao, Q.; Lu, J.; Lauri, G.; Ona, N.; Reagan, E. K.; Ni, H.; Weissman, D.; Percec, V. Targeted Delivery of mRNA with One-Component Ionizable Amphiphilic Janus Dendrimers. *J. Am. Chem. Soc.* **2021**, *143*, 17975−17982.
(67) Lu, J.; Atochina-Vasserman, E. N.; Maurya, D. S.; Sahoo, D.; Ona, N.; Reagan, E. K.; Ni, H.; Weissman, D.; Percec, V. Targeted and Equally Distributed Delivery of mRNA to Organs with Pentaerythritol-Based One-Component Ionizable Amphiphilic Janus Dendrimers. *J. Am. Chem. Soc.* **2023**, *145*, 18760−18766.
(68) Torre, P.; Xiao, Q.; Buzzacchera, I.; Sherman, S. E.; Rahimi, K.; Kostina, N. Y.; Rodriguez-Emmenegger, C.; Möller, M.; Wilson, C. J.; Klein, M. L.; Good, M. C.; Percec, V. Encapsulation of hydrophobic components in dendrimersomes and decoration of their surface with proteins and nucleic acids. *Proc. Natl. Acad. Sci. U.S.A.* **2019**, *116*, 15378−15385.
(69) Joseph, A.; Wagner, A. M.; Garay-Sarmiento, M.; Aleksanyan, M.; Haraszti, T.; Söder, D.; Georgiev, V. N.; Dimova, R.; Percec, V.; Rodriguez-Emmenegger, C. Zwitterionic Dendrimersomes: A Closer Xenobiotic Mimic of Cell Membranes. *Adv. Mater.* **2022**, *34*, 2206288.
(70) Wagner, A. M.; Eto, H.; Joseph, A.; Kohyama, S.; Haraszti, T.; Zamora, R. A.; Vorobii, M.; Giannotti, M. I.; Schwille, P.; Rodriguez-Emmenegger, C. Dendrimersome Synthetic Cells Harbor Cell Division Machinery of Bacteria. *Adv. Mater.* **2022**, *34*, 2202364.
(71) Xiao, Q.; Zhang, S.; Wang, Z.; Sherman, S. E.; Moussodia, R.-O.; Peterca, M.; Muncan, A.; Williams, D. R.; Hammer, D. A.; Vértesy, S.; André, S.; Gabius, H.-J.; Klein, M. L.; Percec, V. Onion-like glycodendrimersomes from sequence-defined Janus glycodendrimers and influence of architecture on reactivity to a lectin. *Proc. Natl. Acad. Sci. U.S.A.* **2016**, *113*, 1162−1167.
(72) Kopitz, J.; Xiao, Q.; Ludwig, A. K.; Romero, A.; Michalak, M.; Sherman, S. E.; Zhou, X.; Dazen, C.; Vértesy, S.; Kaltner, H.; Klein, M. L.; Gabius, H. J.; Percec, V. Reaction of a Programmable Glycan Presentation of Glycodendrimersomes and Cells with Engineered Human Lectins To Show the Sugar Functionality of the Cell Surface. *Angew. Chem.* **2017**, *129*, 14869−14873.
(73) Ludwig, A.-K.; Michalak, M.; Xiao, Q.; Gilles, U.; Medrano, F. J.; Ma, H.; Fitzgerald, F. G.; Hasley, W. D.; Melendez-Davila, A.; Liu, M.; Rahimi, K.; Kostina, N. Y.; Rodriguez-Emmenegger, C.; Möller, M.; Lindner, I.; Kaltner, H.; Cudic, M.; Reusch, D.; Kopitz, J.; Romero, A.; Oscarson, S.; Klein, M. L.; Gabius, H.-J.; Percec, V. Design-functionality relationships for adhesion/growth-regulatory galectins. *Proc. Natl. Acad. Sci. U.S.A.* **2019**, *116*, 2837−2842.
(74) Xiao, Q.; Ludwig, A.-K.; Romanò, C.; Buzzacchera, I.; Sherman, S. E.; Vetro, M.; Vértesy, S.; Kaltner, H.; Reed, E. H.; Möller, M.; Wilson, C. J.; Hammer, D. A.; Oscarson, S.; Klein, M. L.; Gabius, H.-J.; Percec, V. Exploring functional pairing between surface glycoconjugates and human galectins using programmable glycodendrimersomes. *Proc. Natl. Acad. Sci. U.S.A.* **2018**, *115*, E2509−E2518.
(75) Zhang, S.; Moussodia, R.-O.; Murzeau, C.; Sun, H.-J.; Klein, M. L.; Vértesy, S.; André, S.; Roy, R.; Gabius, H.-J.; Percec, V. Dissecting Molecular Aspects of Cell Interactions Using Glycodendrimersomes with Programmable Glycan Presentation and Engineered Human Lectins. *Angew. Chem.* **2015**, *127*, 4108−4112.
(76) Zhang, S.; Moussodia, R.-O.; Vértesy, S.; André, S.; Klein, M. L.; Gabius, H.-J.; Percec, V. Unraveling functional significance of natural variations of a human galectin by glycodendrimersomes with programmable glycan surface. *Proc. Natl. Acad. Sci. U.S.A.* **2015**, *112*, 5585−5590.
(77) Zhang, S.; Xiao, Q.; Sherman, S. E.; Muncan, A.; Ramos Vicente, A. D. M.; Wang, Z.; Hammer, D. A.; Williams, D.; Chen, Y.; Pochan, D. J.; Vértesy, S.; André, S.; Klein, M. L.; Gabius, H.-J.; Percec, V. Glycodendrimersomes from Sequence-Defined Janus Glycodendrimers Reveal High Activity and Sensor Capacity for the Agglutination by Natural Variants of Human Lectins. *J. Am. Chem. Soc.* **2015**, *137*, 13334−13344.
(78) Calero, C.; Franzese, G. Membranes with different hydration levels: The interface between bound and unbound hydration water. *J. Mol. Liq.* **2019**, *273*, 488−496.

https://doi.org/10.1021/acs.biomac.3c01027
Biomacromolecules 2024, 25, 366−378

(79) Calero, C.; Stanley, H.; Franzese, G. Structural Interpretation of the Large Slowdown of Water Dynamics at Stacked Phospholipid Membranes for Decreasing Hydration Level: All-Atom Molecular Dynamics. *Materials* **2016**, *9*, 319.
(80) Martelli, F.; Crain, J.; Franzese, G. Network Topology in Water Nanoconfined between Phospholipid Membranes. *ACS Nano* **2020**, *14*, 8616−8623.
(81) Zhang, S.; Sun, H.-J.; Hughes, A. D.; Draghici, B.; Lejnieks, J.; Leowanawat, P.; Bertin, A.; Otero De Leon, L.; Kulikov, O. V.; Chen, Y.; Pochan, D. J.; Heiney, P. A.; Percec, V. "Single-Single" Amphiphilic Janus Dendrimers Self-Assemble into Uniform Dendrimersomes with Predictable Size. *ACS Nano* **2014**, *8*, 1554−1565.
(82) Radja, A.; Horsley, E. M.; Lavrentovich, M. O.; Sweeney, A. M. Pollen Cell Wall Patterns Form from Modulated Phases. *Cell* **2019**, *176*, 856−868.e10.
(83) Curk, T.; Dobnikar, J.; Frenkel, D. *Design Principles for Super Selectivity Using Multivalent Interactions*; John Wiley & Sons, Ltd, 2017; pp 75−101.
(84) Dubacheva, G. V.; Curk, T.; Frenkel, D.; Richter, R. P. Multivalent Recognition at Fluid Surfaces: The Interplay of Receptor Clustering and Superselectivity. *J. Am. Chem. Soc.* **2019**, *141*, 2577−2588.
(85) Martinez-Veracoechea, F. J.; Frenkel, D. Designing super selectivity in multivalent nano-particle binding. *Proc. Natl. Acad. Sci. U.S.A.* **2011**, *108*, 10963−10968.

https://doi.org/10.1021/acs.biomac.3c01027
Biomacromolecules 2024, 25, 366−378